Electronic Supplementary Information

Borate-driven ionic rectifiers based on sugar-bearing single nanochannels

Vanina M. Cayón, [†1] Gregorio Laucirica,[†1] Yamili Toum Terrones,[1] M. Lorena Cortez,[1] Gonzalo Pérez-Mitta, [1] Jun Shen,[2] Christian Hess,[2] María Eugenia Toimil-Molares,[3] Christina Trautmann,[3,4] Waldemar A. Marmisollé[1]* and Omar Azzaroni[1]*

[1]Instituto de Investigaciones Fisicoquímicas Teóricas y Aplicadas (INIFTA), Departamento de Química, Facultad de Ciencias Exactas, Universidad Nacional de La Plata, CONICET – CC 16 Suc. 4, 1900 La Plata, Argentina

[2]Eduard-Zintl-Institut für Anorganische und Physikalische Chemie, Technische Universität Darmstadt, Alarich-Weiss-Str. 8, Darmstadt, Germany

[3]GSI Helmholtzzentrum für Schwerionenforschung, 64291 Darmstadt, Germany

[4]Technische Universität Darmstadt, Materialwissenschaft, 64287 Darmstadt, Germany

[†] These authors contributed equally to the work

E-mail: wmarmi@inifta.unlp.edu.ar (W.A.M.)

E-mail: azzaroni@inifta.unlp.edu.ar (O.A.)

Geometrical characterization by Scanning Electron Microscopy (SEM)

Bullet-shaped PET nanochannels were characterized by SEM (**Figure S1**). For this, an irradiated PET foil (fluence of 10^9 ions/cm^2) that had been subjected to an asymmetrical surfactant-assisted etching was positioned at 90º.[1] In order to obtain the cross-section images, a special freeze-fracture technique was used to render the polymer brittle. The technique includes the photo oxidation degradation of the polymer.[2] Under predetermined conditions for the degradation reaction, it is possible to change the mechanical properties of a polymer, keeping the sample morphology unaltered. Techniques based on ultraviolet radiation (UV) and photo oxidation degradation are appropriate for PET. This polymer has in its structure macromolecules that contain aromatic chains, that confer radiation resistance. In this context, with a suitable selection of the wavelength (λ), in the degradation of thin (5–10 μm thick) samples can be achieved of good results. The PET transmission cut-off for electromagnetic radiation corresponds to λ = 313 nm. A shorter wavelength is absorbed only by a thin surface layer and does not actually affect the deeper polymer layers, whereas λ > 320 nm is absorbed barely by PET molecules and, hence, fails to initiate the degradation. So, PET samples were irradiated at wavelength of 310–320 nm. To achieve a more homogeneous degradation in depth, both surfaces of the sample were exposed to UV light. This imply the degradation of the polymer under the exposure to soft UV light for 35hs and then fractured at liquid nitrogen temperature.[3] The channels exhibited a typical bullet profile in the tip region (**Figure S3(a)**). Moreover, base and tip diameters of around ~900 and ~70 nm were determined respectively (**Figure S3(a)**).

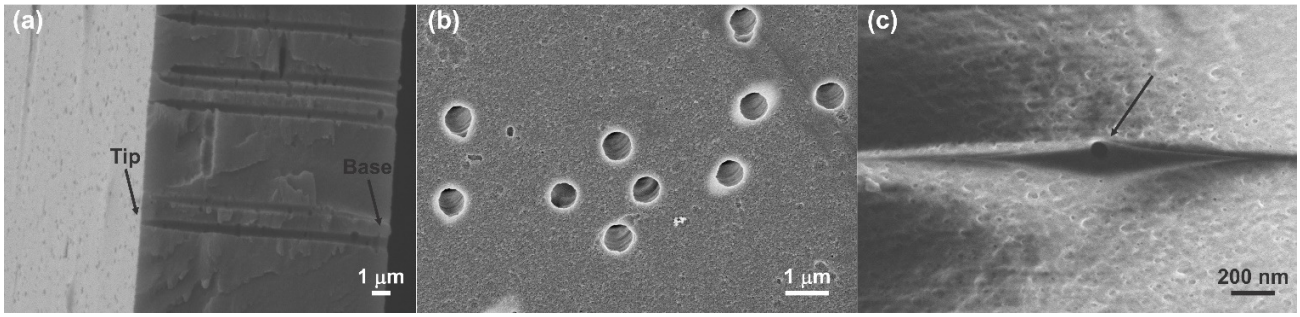

Figure S1. SEM micrograph of (a) cross-section, (b) base and (c) tip side of the bullet-shaped PET nanochannels.

Then, the experimental base diameter (D) was used to calculate the effective tip diameter (d_{tip}) of the PET/SiO_2 SSN. In particular, d_{tip} was estimated from the conductimetric measurement in 0.1 M KCl at pH=4 (at which the SSNs present a ohmic behavior) to be d_{tip}~ 27 nm, using the following equation **(1)** for bullet-shaped channels:[4,5]

$$R = \frac{1}{\pi\kappa}\int_0^L \frac{dx}{\left[\frac{D}{2} - \left(\frac{D-d_{tip}}{2}\right)exp(-x/h)\right]^2} \quad \textbf{(1)}$$

where R is the electrical resistance measured at low potential transmembrane voltage (-0.1 V< V_t< 0.1 V), κ is the specific conductance of 0.1 M KCl at 25°C (~0.0128 S/cm), L means the nanochannel length corresponding to the thickness of the foil (12 μm) and h is a geometrical parameter related to the curvature of the bullet-shaped nanochannel. The parameter h was set to 1500 nm based on previous results for this type of SSNs.[6] Discrepancies between the tip diameter estimated by electrochemical measurement and the tip diameter determined by SEM images can be ascribed to both the diminution in the tip diameter due to the SiO_2 coating and variations sample-to-sample in the nanofabrication.

pH and ionic strength effects in PET/SiO_2 SSN

To characterize the PET/SiO_2 SSN surface and optimize the measurement conditions, different electrolyte concentrations and pH were explored for the *I-V* curves (**Figure S2**) As confirmed from data in **Figure S2 (a)**, at pH 7, silanol groups in the channel walls are non-protonated, the surface is negatively charged and the pore rectifies the ion current in a cation-driven regime. In contrast, at pH 4 silanol groups are partially protonated and the silica surface is less charged. In terms of the *I-V* curve, this implies a practically ohmic behavior.

At pH 7, an increment in the ionic strength triggers a remarkable enhancement in the transmembrane current at +1 V (**Figure S2 (b)**) keeping the diode-like behavior.

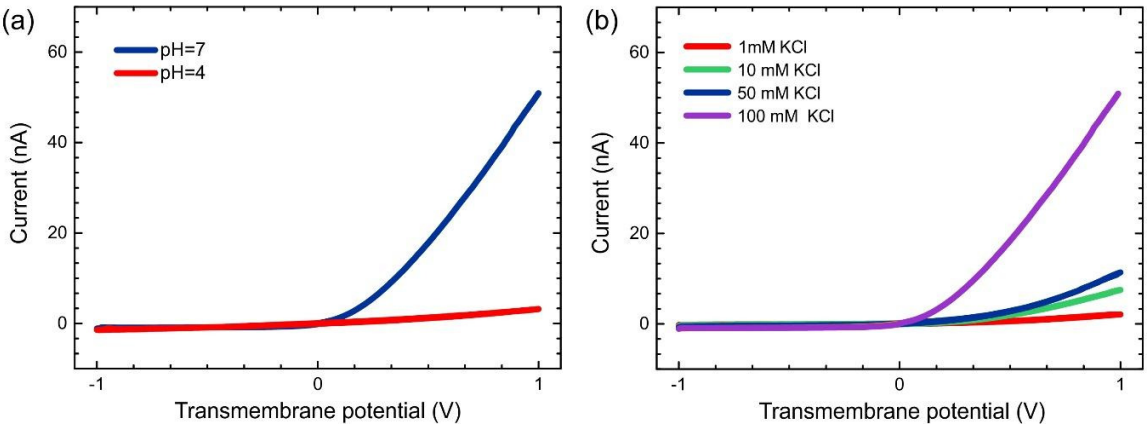

Figure S2. **(a)** Experimental *I-V* curves of the PET/SiO_2 nanochannel at different pH conditions and 0.1 M KCl. **(b)** Experimental curves of the PET/SiO_2 nanochannel at different KCl concentrations at pH 7.

Iontronic characterization of a PET SSN

In terms of ion transport properties, bullet-shaped PET SSNs evidence a cation-driven rectification (f_{rec} = -18.8) owing to the interplay between the negative surface charge generated by the dissociation of carboxyl groups at neutral pH and the asymmetrical shape of the nanochannel (**Figure S3**).

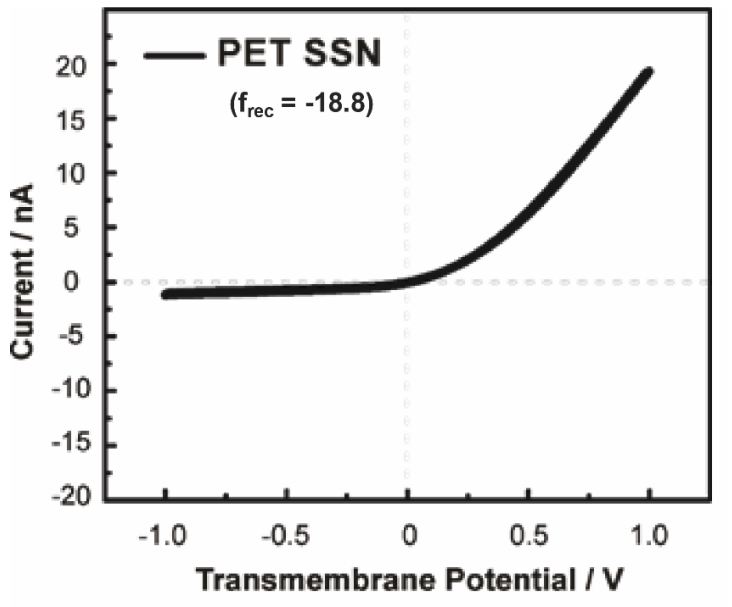

Figure S3. *I-V* curve (0.1 M KCl solution, pH=7) for the bare PET SSN.

X-ray photoelectron spectroscopy (XPS):

With the aim to characterize the surface composition, the PET/SiO_2-Glu modified membrane was analyzed by XPS measurements. XPS spectra of a PET/SiO_2-Glu modified membrane and the assignment of the characteristic peaks are displayed in **Figure S4 (a)** and **(b)**. The XPS characterization confirms the surface modification and data are in good agreement with previous reports.[7,8]

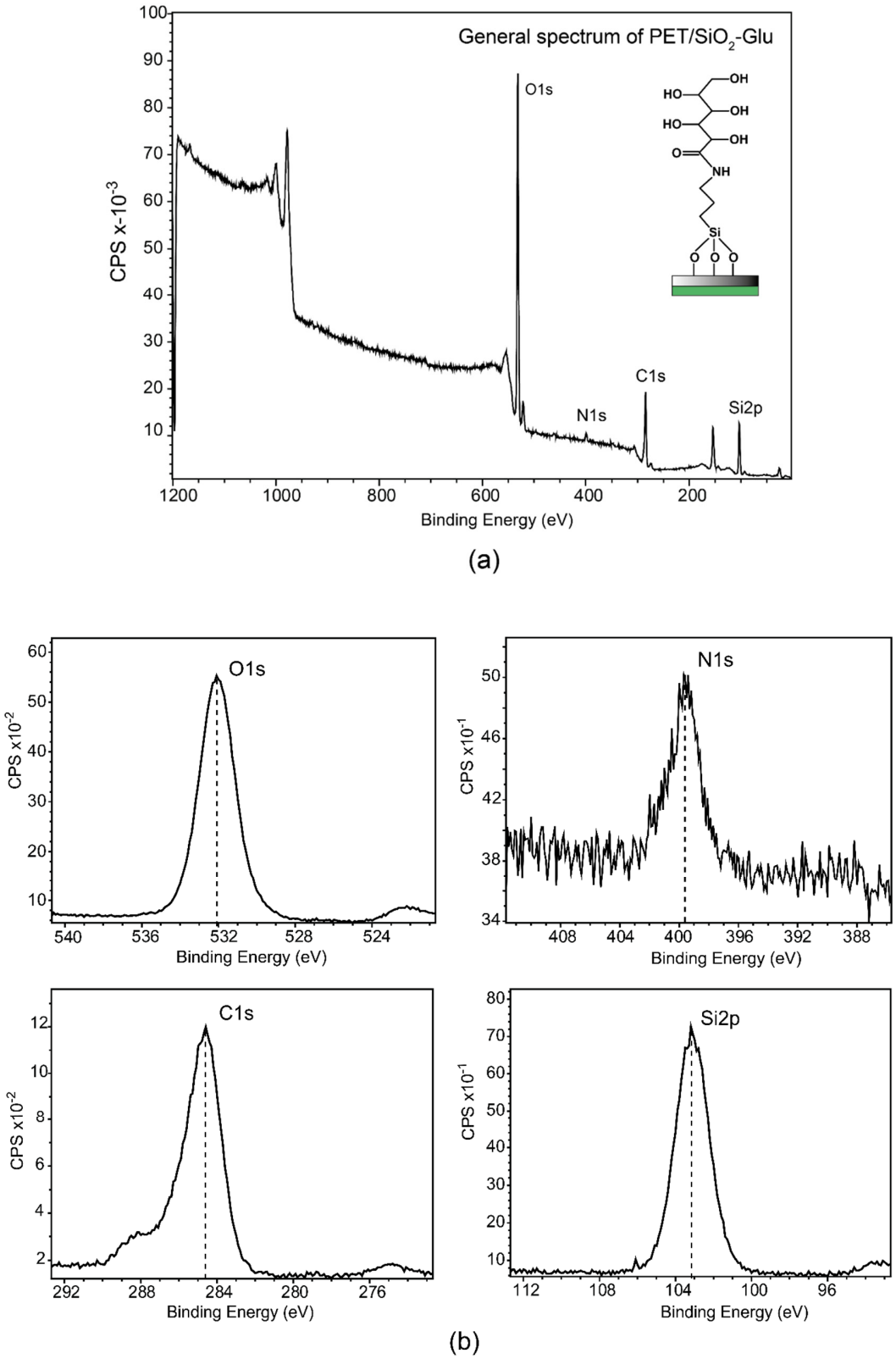

Figure S4. (a) XP general spectrum of the PET/SiO_2-Glu modified membrane. **(b)** Zoom-in the corresponding O 1s, N 1s, C1s and Si 2p peak regions. The binding energies are indicated by vertical dashed lines.

Boric acid, borate and boroesters

The ability of boronic and boric acids to bind with diols was first recognized over a century ago. Now it is accepted that the interaction between boronic acid and a diol is known to be one of the strongest single-pair reversible functional group interactions in an aqueous environment.[9] As shown in ¡Error! No se encuentra el origen de la referencia., the pKa of boric acid is 9.2, and the presence of borate anion is favored at basic pH.[10] Boric acid, $B(OH)_3$, is a trigonal planar molecule, and the tetrahydroxyborate complex or borate anion $[B(OH)_4]^-$ presents a tetrahedral geometry. Once borate has been formed, 1,2 or 1,3-diols can replace hydroxyl groups to give boroesters in a reversible way and at acidic pH, the boroester can turn back to boric acid.

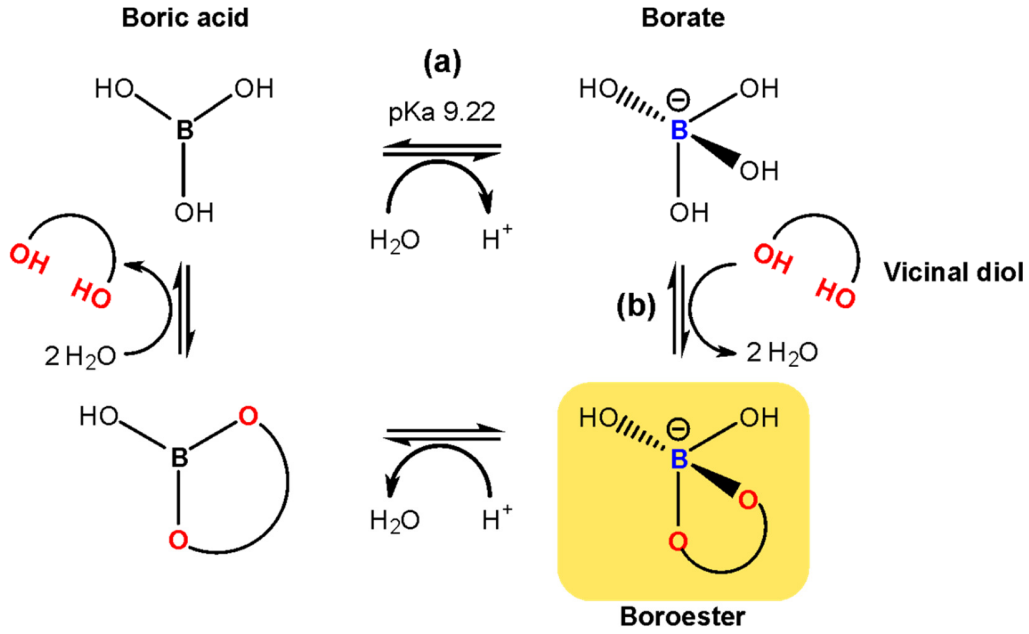

Figure S5. Scheme depicting the boric acid/borate equilibrium and the vicinal diol interaction to form boroesters, depending on pH.

Control experiments: the effect of borate anion in PET/SiO_2 SSN

To rule our non-specific effects of the high borate concentrations in the *I-V* measurements, *I-V* curves for the unmodified PET/SiO_2 SSN samples in the absence and in the presence of the borate anions. **Figure S6** reveals that exposure to 100 mM boric acid did not generate appreciable changes in the iontronic signal, which reinforces the idea that borate does not interact with the PET/SiO_2 surface under the working conditions and, therefore, the iontronic changes obtained for PET/SiO_2/Glu SSN in presence of borate are explained in terms of the sugar-borate interaction.

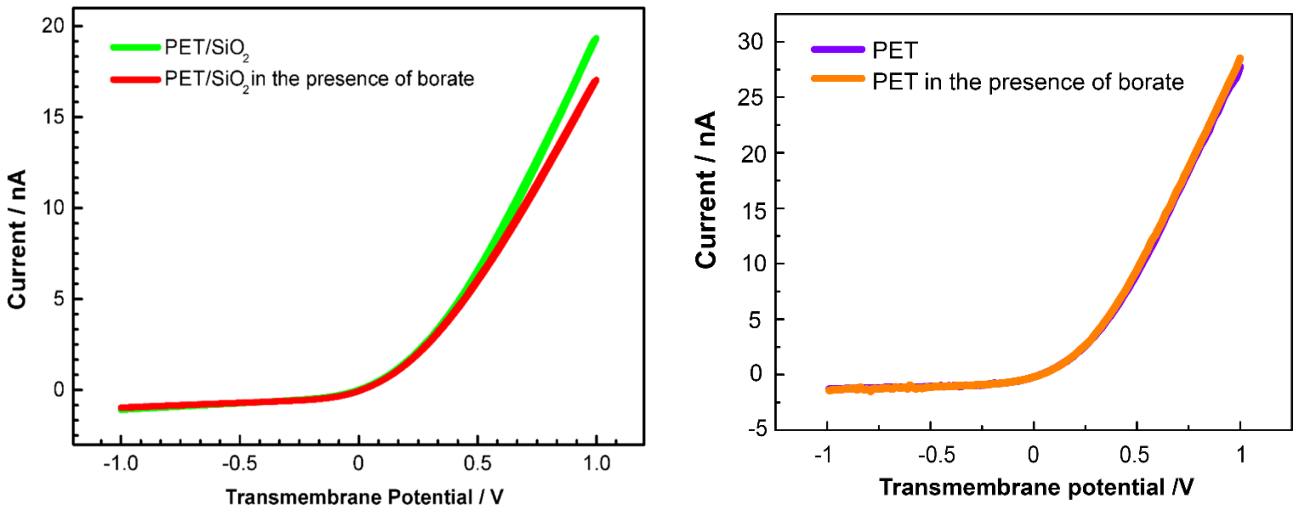

Figure S6. Control experiments. Left: *I-V* curves for PET/SiO_2 SSN (green line) and PET/SiO_2 SSN in the presence of borate (100 mM boric acid, red line); Right: *I-V* curves for the bare PET channel (violet line) and PET channel in the presence of borate (100 mM boric acid, orange line).

On the other hand, analysis of the current as a function of the measurement time was carried out for the PET/SiO_2/Glu/Borate nanochannel system. **Figure S7** shows good current stability (in the presence and absence of borate) upon sweeping transmembrane potential between -1 V and +1 V.

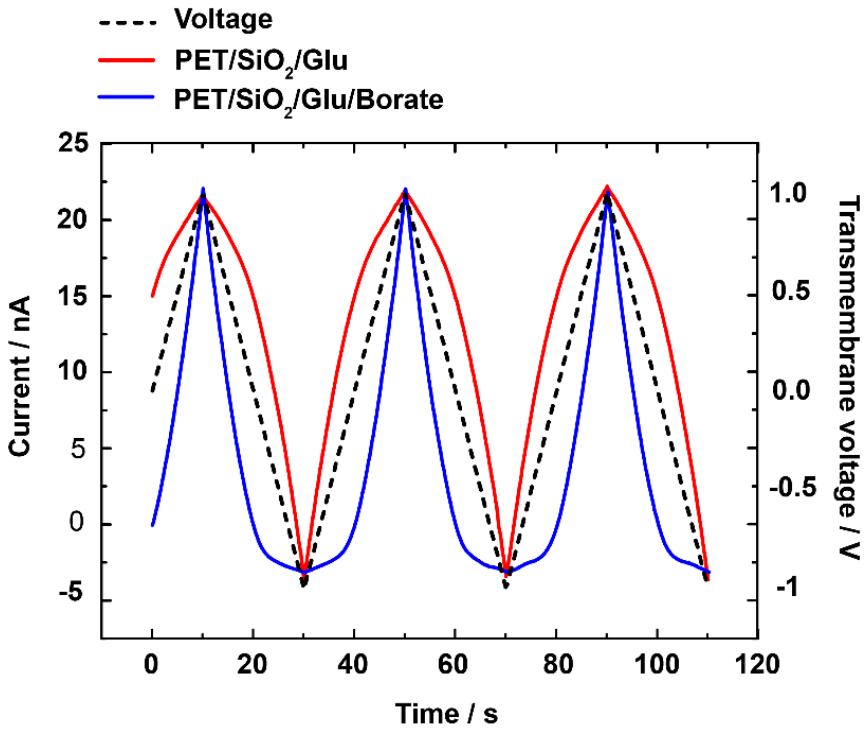

Figure S7. Current measurements expressed in terms of time. Dashed black line indicates the variation in the transmembrane voltage applied.

Binding Model for Borate Responsiveness

For interpreting the borate-responsiveness of the PET/SiO_2-Glu SSN, we adapted a previously developed binding model to the present case.[11] The general binding scheme is depicted in **Scheme S1**.

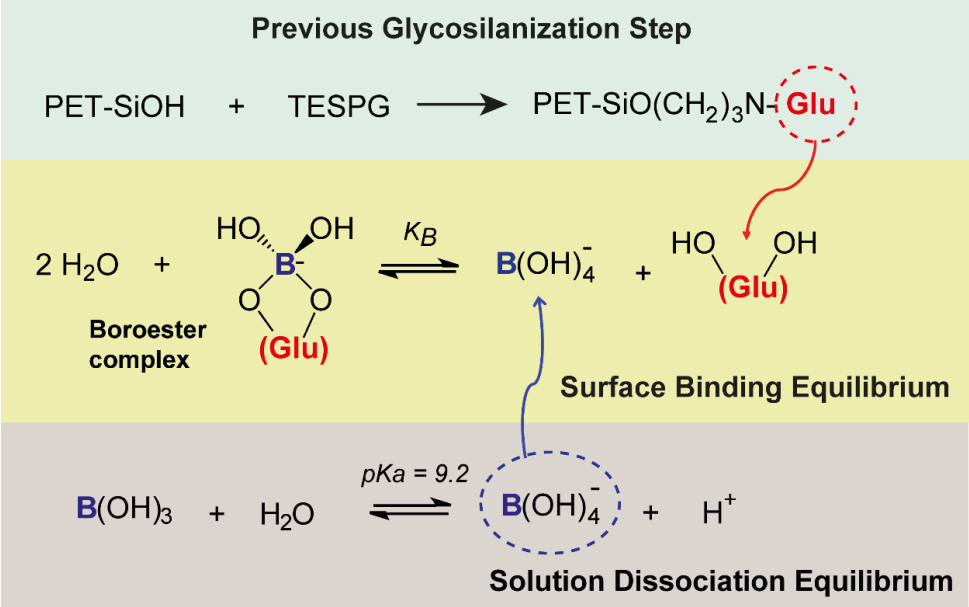

Scheme S1. Brief description of the functionalization and binding equilibrium processes taking place in the system.

After the functionalization step with TESPG (**Scheme S1**), a fraction of the silanol groups on the surface of the SiO_2 layer is covalently (irreversibly) bound to silane groups TESPG. We refer to this surface carbohydrate-like moiety as (Glu).

As the boroester formation is ascribed to be produced from the borate anion,[12,13] the dissociation equilibrium of boric acid needs to be firstly considered:

$$B(OH)_3 + H_2O \leftrightarrow B(OH)_4^- + H^+ \qquad K_a = \frac{[B(OH)_4^-][H^+]}{[B(OH)_3]} \qquad \textbf{(S.1)}$$

Reported values for this pK_a are around 9.2, while they also depend on the salinity conditions.[10] Although other dimeric and polymeric borates can be formed at higher pH, keeping the pH around 7 allows just considering both $B(OH)_3$ and $B(OH)_4^-$ species. Particularly, it is possible to account for the dissociation degree α:

$$\alpha = \frac{\left[B(OH)_4^-\right]}{\left[B(OH)_4^-\right] + \left[B(OH)_3\right]} = \frac{\left[B(OH)_4^-\right]}{C_B} \qquad \textbf{(S.2)}$$

where C_B means the boric acid analytical concentration. This fraction is dependent on pH according to **Eq. (S.1)**. On the other hand, the binding of borate to the glycol groups on the nanochannel surface can be considerer as[12]:

$$(Glu)(OH)_2 + B(OH)_4^- \leftrightarrow -(Glu)O_2B\left(OH\right)_2^- + 2H_2O \qquad \textbf{(S.3)}$$

where $(Glu)(OH)_2$ and $(Glu)O_2B\left(OH\right)_2^-$ means the free surface glycol residues and bound surface glycol residues, respectively (**Scheme S1**). For this interaction, a simple binding constant can be defined as

$$K_B = \frac{\left[(Glu)O_2B\left(OH\right)_2^-\right]}{\left[(Glu)(OH)_2\right]\left[B(OH)_4^-\right]} \qquad \textbf{(S.4)}$$

being $\left[(Glu)(OH)_2\right]$ and $\left[(Glu)O_2B\left(OH\right)_2^-\right]$ surface concentrations and $\left[B(OH)_4^-\right]$ the borate bulk concentration.

Being the total surface concentration of glycosyl moieties constant, $\left[(Glu)\right]$, (and determined in the previous functionalization step), the mass balance allows writing:

$$\left[(Glu)\right] = \left[(Glu)(OH)_2\right] + \left[(Glu)O_2B\left(OH\right)_2^-\right] \qquad \textbf{(S.5)}$$

Then,

$$\left[(Glu)O_2B\left(OH\right)_2^-\right] = \frac{K_B\left[B(OH)_4^-\right]\left[(Glu)\right]}{1 + K_B\left[B(OH)_4^-\right]} \qquad \textbf{(S.6)}$$

On the other hand, the presence of negative charges coming from unmodified surface SiO- groups could also contribute to the surface charge.[14] Thus, the surface charge density (σ) can be computed by taking into account the contribution of negatively charged boroester complexes and the residual silanol groups,

$$\sigma \propto -\left(\left[(Glu)O_2B\left(OH\right)_2^-\right] + \left[SiO^-\right]\right) \qquad \textbf{(S.7)}$$

By employing relation **(S.6)**, it results

$$\sigma \propto -\left(\frac{K_B\left[B(OH)_4^- \right]\left[(Glu) \right]}{1+K_B\left[B(OH)_4^- \right]} + \left[SiO^- \right] \right) \qquad \textbf{(S.8)}$$

In the absence of borate in solution, the surface charge is due to the free silanol groups:

$$\sigma_0 \propto -\left[SiO^- \right] \qquad \textbf{(S.9)}$$

Then:

$$\sigma - \sigma_0 \propto -\left(\frac{K_B\left[B(OH)_4^- \right]\left[(Glu) \right]}{1+K_B\left[B(OH)_4^- \right]} \right) \qquad \textbf{(S.10)}$$

On the other hand, when the boric concentration is high, practically all glycol groups would be in the form of boroester complexes, so that $\left[(Glu)O_2B\left(OH\right)_2^- \right] = \left[(Glu) \right]$. Then, we can define:

$$\sigma_\infty \propto -\left(\left[(Glu) \right] + \left[SiO^- \right] \right) \qquad \textbf{(S.11)}$$

Then, expression **(S.10)** can be rewritten as follows:

$$\frac{\sigma - \sigma_0}{\sigma_\infty - \sigma_0} = \frac{K_B\left[B(OH)_4^- \right]}{1+K_B\left[B(OH)_4^- \right]} \qquad \textbf{(S.12)}$$

It has been proved that for low surface charge, there is a linear relationship between σ and f_{rec}, [14] which allows writing relative changes in surface charge density in terms of rectification factors as:

$$\frac{\sigma - \sigma_0}{\sigma_\infty - \sigma_0} = \frac{f_{rec} - f_{rec}^0}{f_{rec}^\infty - f_{rec}^0} \qquad \textbf{(S.13)}$$

Then, **Eq (S.12)** can be rewritten as:

$$f_{rec} - f_{rec}^{0} = \left(f_{rec}^{\infty} - f_{rec}^{0} \right) \frac{K_{B'} C_B}{1 + K_{B'} C_B} \qquad \textbf{(S. 14)}$$

Where $K_{B'} = \alpha K_B$ has been defined as an effective binding constant in the operative conditions. Thus, $K_{B'}$ can be determined by fitting $f_{rec} - f_{rec}^{0}$ experimental values as a function of boric acid analytical concentration using **eq. (S.14)**.

References

1 P. Y. Apel, I. V Blonskaya, S. N. Dmitriev, O. L. Orelovitch, A. Presz and B. A. Sartowska, *Nanotechnology*, 2007, **18**, 305302.

2 O. . Orelovitch, P. Y. Apel and B. Sartowska, *Mater. Chem. Phys.*, 2003, **81**, 349–351.

3 O. L. Orelovich and P. Y. Apel', *Instruments Exp. Tech.*, 2001, **44**, 111–114.

4 P. Y. Apel, I. V Blonskaya, O. L. Orelovitch, P. Ramirez and B. A. Sartowska, *Nanotechnology*, 2011, **22**, 175302.

5 P. Y. Apel, I. V. Blonskaya, N. V. Levkovich and O. L. Orelovich, *Pet. Chem.*, 2011, **51**, 555–567.

6 G. Laucirica, A. Albesa, M. E. Toimil-Molares, C. Trautmann, W. Marmisollé and O. Azzaroni, *Nano Energy*, 2020, 104612.

7 N. Sobel, C. Hess, M. Lukas, A. Spende, B. Stühn, M. E. Toimil-Molares and C. Trautmann, *Beilstein J. Nanotechnol.*, 2015, **6**, 472–479.

8 A. Spende, N. Sobel, M. Lukas, R. Zierold, J. C. Riedl, L. Gura, I. Schubert, J. M. M. Moreno, K. Nielsch, B. Stühn, C. Hess, C. Trautmann and M. E. Toimil-Molares, *Nanotechnology*, , DOI:10.1088/0957-4484/26/33/335301.

9 J. Yan, H. Fang and B. Wang, *Med. Res. Rev.*, 2005, **25**, 490–520.

10 M. H. Oo and L. Song, *Desalination*, 2009, **246**, 605–612.

11 G. Laucirica, W. A. Marmisollé and O. Azzaroni, *Phys. Chem. Chem. Phys.*, 2017, **19**, 8612–8620.

12 J. P. Quirino, *Chromatographia*, 2010, **72**, 503–510.

13 S. Hoffstetter-Kuhn, A. Paulus, E. Gassmann and H. Michael Widmer, *Anal. Chem.*, 1991, **63**, 1541–1547.

14 G. Pérez-Mitta, A. Albesa, F. M. Gilles, M. E. Toimil-Molares, C. Trautmann and O. Azzaroni, *J. Phys. Chem. C*, 2017, **121**, 9070–9076.